J. Fluid Mech. (1999), *vol.* 388, *pp.* 289–313. Printed in the United Kingdom

Vortex generation by line plumes in a rotating stratified fluid

By JOHN W. M. BUSH[1]† AND ANDREW W. WOODS[2]

[1] Institute of Theoretical Geophysics, Department of Applied Mathematics and Theoretical Physics, University of Cambridge, Silver Street, Cambridge CB3 9EW, UK

[2] School of Mathematics, University of Bristol, University Walk, Bristol BS8 1TW, UK

(Received 3 November 1997 and in revised form 21 December 1998)

We present the results of an experimental investigation of the generation of coherent vortical structures by buoyant line plumes in rotating fluids. Both uniform and stratified ambients are considered. By combining the scalings describing turbulent plumes and geostrophically balanced vortices, we develop a simple model which predicts the scale of the coherent vortical structures in excellent accord with laboratory experiments.

We examine the motion induced by a constant buoyancy flux per unit length B, released for a finite time t_s, from a source of length L into a fluid rotating with angular speed $\Omega = f/2$. When the plume discharges into a uniformly stratified environment characterized by a constant Brunt–Väisälä frequency, $N > f$, the fluid rises to its level of neutral buoyancy unaffected by the system rotation before intruding as a gravity current. Rotation has a strong impact on the subsequent dynamics: shear develops across the spreading neutral cloud which eventually goes unstable, breaking into a chain of anticyclonic lenticular vortices. The number of vortices n emerging from the instability of the neutral cloud, $n = (0.65 \pm 0.1)Lf^{1/2}/(t_s^{1/2}B^{1/3})$, is independent of the ambient stratification, which serves only to prescribe the intrusion height and aspect ratio of the resulting vortex structures. The experiments indicate that the Prandtl ratio characterizing the geostrophic vortices is given by $P = Nh/(fR) = 0.47 \pm 0.12$, where h and R are, respectively, the half-height and radius of the vortices. The lenticular vortices may merge soon after formation, but are generally stable and persist until they are spun-down by viscous effects.

When the fluid is homogeneous, the plume fluid rises until it impinges on a free surface. The nature of the flow depends critically on the relative magnitudes of the layer depth H and the rotational lengthscale $L_f = B^{1/3}/f$. For $H > 10L_f$, the ascent phase of the plume is influenced by the system rotation and the line plume breaks into a series of unstable anticylonic columns of characteristic radius $(5.3 \pm 1.0)B^{1/3}/f$ which typically interact and lose their coherence before surfacing. When $H < 10L_f$, the system rotation does not influence the plume ascent, but does control the spreading of the gravity current at the free surface. In a manner analogous to that observed in the stratified ambient, shear develops across the surface current, which eventually becomes unstable and generates a series of anticyclonic surface eddies with characteristic radius $(1.6 \pm 0.2)B^{1/3}t_s^{1/3}/f^{2/3}$. These surface eddies are significantly more stable than their columnar counterparts, but less so than the lenticular eddies arising in the uniformly stratified ambient.

† Present address: Department of Mathematics, MIT, 77 Massachusetts Ave., 2-382, Cambridge MA 02139, USA.

The relevance of the study to the formation of coherent vortical structures by leads in the polar ocean and hydrothermal venting is discussed.

1. Introduction

In a number of oceanographic and atmospheric situations, buoyant fluid is released into the aqueous environment from long linear sources and is influenced by both ambient stratification and the Earth's rotation; for example, when brine is rejected from the refreezing of cracks or 'leads' in the polar ice caps (Morison *et al.* 1992), when hydrothermal fluid is released from long cracks on the seafloor generated by tectonic activity in the vicinity of mid-ocean ridges (Baker 1995), and when hot gas is released into the atmosphere by volcanic activity along fissures (Stothers 1989; Woods 1993). We here consider the dynamics of line plumes in rotating fluids, and examine the mechanism by which they generate coherent vortical structures. Particular attention is given to predicting the dimensions of the resulting vortices as a function of the plume source parameters.

Table 1 lists a number of relevant studies of turbulent plumes and thermals emerging from point and line sources. The seminal work on the theory of turbulent plumes is that of Morton, Taylor & Turner (1956), who developed a consistent physical model for turbulent entrainment into plumes. When the ambient is stratified, the plume rises and entrains fluid until it reaches its level of neutral buoyancy where it intrudes as a gravity current or 'neutral cloud'. The influence of rotation on thermals rising from point sources in a homogeneous ambient was considered by Helfrich (1994), who demonstrated that rotation serves to suppress entrainment into the thermal. The influence of rotation on point plumes in homogeneous fluids has recently been examined by Fernando, Chen & Ayotte (1998) and Bush & Woods (1998). Helfrich & Battisti (1991) and Speer & Marshall (1995) have considered the combined influence of stratification and rotation on the dynamics of a point plume. As their study was motivated by the problem of hydrothermal venting in the deep ocean, they considered the case in which the ratio of the Brunt–Väisälä to rotational frequencies N/f was greater than unity. In this case, the plume ascent phase is not influenced by the system rotation, while the spreading phase at the level of neutral buoyancy is: the neutral cloud adjusts to a geostrophic state after a time comparable to the rotation period, with its half-height to radius aspect ratio h/R scaling with N/f, so that the Prandtl ratio $P = Nh/fR$ remains of order unity. Laboratory and numerical investigations (Helfrich & Battisti 1991; Helfrich & Speer 1995) suggest that the neutral cloud continues to expand at its level of neutral buoyancy Z_n for a time $t_i \sim N/f^2$ until it reaches a critical radius NZ_n/f, and goes unstable in one of two manners. For $N/f > 2$, the neutral cloud simply drifts off the source, while for $N/f < 2$, it splits into two vortex dipoles which propagate away from the source. We note that for the case of a finite release of source fluid from a point source for a time $t_s < t_i$, the size of the resulting vortex will depend explicitly on the source time t_s; in particular, the vortex radius will be proportional to $t_s^{1/3}$. In this study, we focus our attention on the analogous problem of a finite time release of fluid from a line source, for which the scale of the emerging vortices depends explicitly on the duration of the release.

The formation of coherent vortical structures is a generic feature of the collapse of turbulent regions in rotating fluids, and so must accompany plume-induced mixing. In a homogeneous ambient the resulting geostrophic flow structures are columnar, while

Ambient	Point source	Line source
Homogeneous	Morton, Taylor & Turner (1956) (P) Scorer (1957) (T) Johari (1992) (T)	Rouse, Yih & Humphreys (1952) (P) Richards (1963) (T)
Stratified	Morton, Taylor & Turner (1956) (P) Noh, Fernando & Ching (1992) (P) Ching, Fernando & Noh (1993) (P)	Wright & Wallace (1979) (P)
Rotating homogeneous	Elrick (1979) (T) Helfrich (1994) (T) Ayotte & Fernando (1994) (T) Fernando, Chen & Ayotte (1998) (P)	Fernando & Ching (1993) (P) Lavelle & Smith (1996) (P) Present study
Rotating stratified	Speer & Marshall (1995) (P) Helfrich & Battisti (1991) (P) Helfrich (1994) (T)	Present study

TABLE 1. Summary of studies on the dynamics of turbulent plumes (P) and thermals (T) in the presence of ambient stratification and/or rotation.

in a stratified ambient they are lenticular with characteristic aspect ratio prescribed by N/f. The number of such structures generated by a turbulent plume is prescribed by their size relative to the plume source. Maxworthy & Narimousa (1994) examined the discharge of negatively buoyant fluid from an areal source in a homogeneous rotating fluid, and demonstrated that a series of quasi-two-dimensional anticyclonic vortices (of characteristic radius $7.5B_0^{1/2}/f^{3/2}$, where B_0 is the surface buoyancy flux per unit area) emerge from beneath the source (see also Whitehead, Marshall & Hufford 1996, and Boubnov & van Heijst 1994). Fernando, Chen & Boyer (1991) and Julien *et al.* (1996) have considered the influence of rotation on turbulent thermal convection, and also identified the presence of columnar structures of comparable scale. A discussion of the physical processes accompanying convectively-driven mixing in rotating stratified fluids is given by Maxworthy (1997).

The line plume problem has received considerable recent attention owing to its relevance in modelling thermohaline convection associated with cracks in the polar ice caps, or 'leads'. Motivated by the problem of lead-induced plumes impinging on the pycnocline at the base of the oceanic mixed layer, Noh, Fernando & Ching (1992) and Ching, Fernando & Noh (1993) undertook experimental studies of line plumes impinging on a density interface, and characterized the rate of ascent as well as the intrusion depth of the plume. Fernando & Ching (1993) carried out an experimental study of line plumes in a homogeneous rotating fluid, and Lavelle & Smith (1996) undertook an analogous numerical study. In both studies, the influence of ambient stratification was neglected, and only a limited range of parameter space was examined, so that the striking coherent flow structures reported here were not identified. While the individual effects of stratification and rotation on the dynamics of line plumes have been investigated, the study presented here represents the first investigation of their combined effects. By analogy with the point plume problem, we anticipate that the line plume in a rotating stratified fluid will rise to its level of neutral buoyancy before intruding as a gravity current which eventually goes unstable under the influence of the system rotation. However, we will observe an important distinction between the point and line plume problems: when the source time is less than the instability time of the neutral cloud for the case of a continuous release, a

single stable vortex will emerge above a point plume, while a chain of vortices will form above a line plume.

Griffiths & Linden (1981*a*, *b*, *c*), Griffiths, Killworth & Stern (1982) and Ivey (1987) have considered the instantaneous and continuous release of buoyant fluid in rotating stratified fluids in a variety of axisymmetric geometries, in particular from point sources, ring sources, cylindrical areal sources and cylindrical annuli. They demonstrate that the axisymmetric geostrophic flows associated with the source fluid spreading at the level of neutral buoyancy typically go unstable to vortices whose horizontal lengthscale is comparable to the Rossby deformation radius, $R = Nh/f$, where h is the initial depth of the source fluid. While the instability which they describe is closely related to that arising in the instability of the neutral cloud above a line plume, there are two important differences. First, entrainment into the line plume generates a cyclonic flow beneath the neutral cloud, and thus a vertical shear at its base. Second, the vertical extent of the neutral cloud above a line plume increases with time as the source persists. We here determine the wavelength of instability of the neutral cloud above a line plume as a function of the plume source conditions.

We present the results of an experimental study of turbulent line plumes in a rotating fluid, and give particular attention to the coherent vortical flow structures which emerge from the flow. In § 2, we define the physical system to be considered, and describe our experimental technique. In § 3, we describe the problem of line plumes discharging into a stratified ambient. The homogeneous ambient is considered in § 4. The relevance of the study to the convective motions associated with polar leads and the formation of megaplumes by hydrothermal venting is discussed in § 5.

2. Physical picture

We consider a line source of length L discharging buoyant fluid of density ρ from the base ($z = 0$) of a tank of fluid which is rotating uniformly with angular speed $\Omega = f/2$. For a time t_s, the source discharges a volume flux per unit length Q, and a buoyancy flux per unit length of $B = g'Q$, where $g' = g(\rho - \rho_0)/\rho$ and ρ_0 is the ambient density at the base of the tank. The discharged fluid rises as a turbulent plume, entraining ambient fluid as it rises. Both stratified and homogeneous ambients are considered. In the former case, the stratification is described by a constant Brunt–Vaisala frequency $N = \left(-(g/\rho)(\mathrm{d}\rho/\mathrm{d}z)\right)^{1/2}$, and the plume fluid rises to its level of neutral buoyancy before intruding as a gravity current. We give particular attention to the case of $N/f > 1$, which is relevant in most oceanographic problems. For the case of a homogeneous ambient, the fluid rises until it impinges on a free surface a distance H from the source.

The nature of the flow changes according to the relative magnitudes of the source time t_s, the rotation period $t_f = 1/f$, and the rise time of the plume t_r. When the source time is significantly less than the rise time, $t_s \ll t_r$, the released fluid may be described as a line thermal. While the scaling governing the thermal problem is discussed in the Appendix, we focus our experimental study on the case in which the source time exceeds the rise time, so that the released fluid may be described as a starting plume (Turner 1973). However, we note that our source is terminated after a finite time t_s; consequently, our situation would be most accurately described as a 'starting and stopping plume'. When the rise time of the plume is less than a rotation period, the system rotation has little impact on the ascent phase. In § 3, we consider the case where the line plume rises to its level of neutral buoyancy in a stratified fluid

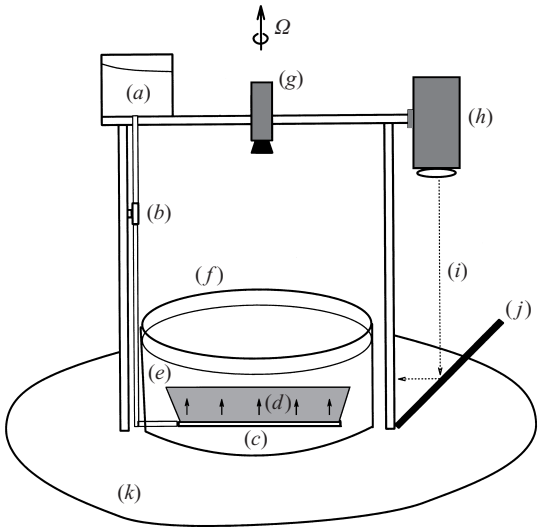

FIGURE 1. A schematic illustration of the experimental apparatus, which consists of (*a*) a reservoir of dyed source fluid, (*b*) a flowmeter, (*c*) a line source, (*d*) a buoyant line plume, (*e*) a salt-stratified or homogeneous ambient in (*f*) a Plexiglas tank, (*g*) a video camera, (*h*) an arc lamp which generates (*i*) a vertical light sheet which is diverted into the horizontal by (*j*) a mirror, and (*k*) a turntable.

before being influenced by the system rotation. In § 4, we examine a line plume rising through a homogeneous environment, and consider separately the cases in which the ascent phase is and is not influenced by the system rotation.

The experimental apparatus is illustrated in figure 1. A line source, consisting of a piece of copper tubing with a series of colinear 1 mm diameter holes placed 5 mm apart, is attached to the base of a cylindrical Plexiglas tank, of radius 80 cm and depth 40 cm, which is mounted on a turntable. The tank is filled with either a homogeneous or stratified saltwater solution. In the latter case, the tank is filled through a floating sponge using the double bucket technique while the table is rotating in order to ensure a smooth stratification. Once the ambient attains a state of solid body rotation, the source is initiated. Fresh water dyed with fluorescein is gravity-fed for a time t_s to the line source from a reservoir mounted on the top of the rotating table, and the inflow rate monitored by a flowmeter.

The flow is visualized by a horizontal light sheet which illuminates the plume at the spreading level, and captured on video by a camera corotating with the tank. Occasionally, a vertical section was illuminated by the light sheet and captured on video. In a number of experiments involving plume discharge into a homogeneous ambient, the surface motions were made visible by plyolite particles suspended on the free surface. The surface flows could then be resolved by particle-tracking with DigImage, a digital image processing system (Dalziel 1992). Experiments were carried out over a broad range of parameter space, with L varying between 20 and 44 cm, t_s between 10 and 120 s, f between 0.2 and 2 s^{-1}, N between 0.0 and 1.0 s^{-1}, Q between 0.05 and 0.23 $cm^2\,s^{-1}$ and B between 1.0 and 14.0 $cm^3\,s^{-3}$. The details of all of the experiments performed are reported in tables 2–4.

3. Stratified ambient ($N > f$)

We first consider the case of a line plume rising in a stratified environment. When the ascent phase is not influenced by rotation, the flow variables of a two-dimensional

Expt	N (s^{-1})	f (s^{-1})	L (cm)	QL (cm^2 s^{-1})	B (cm^3 s^{-3})	t_s (s)	$Z_n + L_a$ (cm)	P	n	t_w (s)
2-1	0.97	2.0	43.5	4.3	3.04	30	6.5	0.36	6	14
2-2	0.83	2.0	43.5	4.6	2.09	30	6.0	0.5	6	15
2-4	0.82	1.0	43.5	4.6	2.09	30	7.0	0.55	4	24
2-5	0.84	0.6	43.5	4.6	2.09	40	7.0	0.47	3	28
2-7	0.82	0.4	43.5	4.6	2.09	45	8.0	0.37	2	30
2-8	0.82	1.5	43.5	4.6	2.09	25	6.5	0.55	6	20
3-1	0.78	1.0	20.5	3.2	3.06	30	7.5	0.39	2	28
3-2	0.81	0.4	20.5	3.2	3.06	30	7.5	0.41	2	40
8-1	0.81	1.24	40.0	4.6	2.3	20	7.0	0.46	5	—
8-3	0.81	0.8	40.0	4.6	2.3	22	7.0	0.44	$3\frac{1}{2}$	—
8-4	0.81	0.46	20.0	4.6	4.6	15	7.0	0.53	1	30
8-6	0.81	0.46	20.0	4.6	4.6	30	7.0	0.51	1	30
8-8	1.4	0.86	20.0	4.6	4.6	30	8.0	0.54	2	27
13-1	0.9	1.2	42.0	4.6	2.59	30	7.0	0.43	$4\frac{1}{2}$	32
13-2	0.85	1.0	42.0	4.6	2.38	30	7.0	0.49	4	28
13-3	0.8	1.0	42.0	4.6	2.16	30	7.0	0.45	4	30
13-4	0.86	1.0	42.0	4.6	2.59	30	7.0	0.49	$3\frac{1}{2}$	30
13-5	0.86	1.7	42.0	4.6	2.38	30	7.0	0.54	5	20
14-1	0.81	2.0	40.0	4.6	2.27	60	7.0	—	3	21
14-2	0.81	2.2	40.0	4.6	2.27	20	7.0	—	6	15
14-3	0.81	1.2	40.0	4.6	2.27	25	7.0	0.45	4	25
14-4	0.81	2.0	40.0	4.6	2.27	20	7.0	—	6	20

TABLE 2. Experimental data for line plumes rising in a rotating stratified fluid. The neutral cloud intrudes at a height $Z_n + L_a$ above the source before breaking into n vortices characterized by a Prandtl ratio $P = Nh/fR$. The waveform corresponding to the final wavelength of instability first appeared a time t_w after plume initiation.

line plume depend uniquely on the buoyancy flux B and ambient stratification N. In particular, the rise height Z_n, the mean vertical plume speed w, as well as the volume flux per unit length $Q(Z_n)$ and mean buoyancy $g'(Z_n)$ of fluid supplied to the neutral cloud scale as

$$Z_n \sim \frac{B^{1/3}}{N}, \quad w \sim B^{1/3}, \quad Q(Z_n) \sim \frac{B^{2/3}}{N}, \quad g'(Z_n) \sim B^{1/3}N, \tag{3.1}$$

provided that the source length $L \gg Z_n$. The rise time is thus given by $t_r \sim Z_n/w \sim N^{-1}$, so that during ascent the dynamic influence of rotation is negligible provided $N/f \gg 1$.

The neutral heights in our experiments (reported in table 2) were described by $Z_n = (3.0 \pm 1.0)B^{1/3}/N$ in accordance with (3.1), and were not noticeably influenced by the system rotation. This coefficient is not inconsistent with the value of 2.5 reported in Wright & Wallace's (1979) study of line plumes in a stratified non-rotating ambient. The large error reported is associated with uncertainty in the extent of the adjustment length of the turbulent plumes in our experiments (see § 4.3).

Figure 2 illustrates the evolution of the neutral cloud above a line plume in a rotating stratified fluid as viewed from an oblique angle. The plume fluid rises to its level of neutral buoyancy where it spreads as a gravity current. The subsequent dynamics is influenced by rotation: as the long gravity current corresponding to the neutral cloud expands, the Coriolis force acts to drive an anticyclonic flow perpendicular to the spreading direction, and an associated horizontal shear across

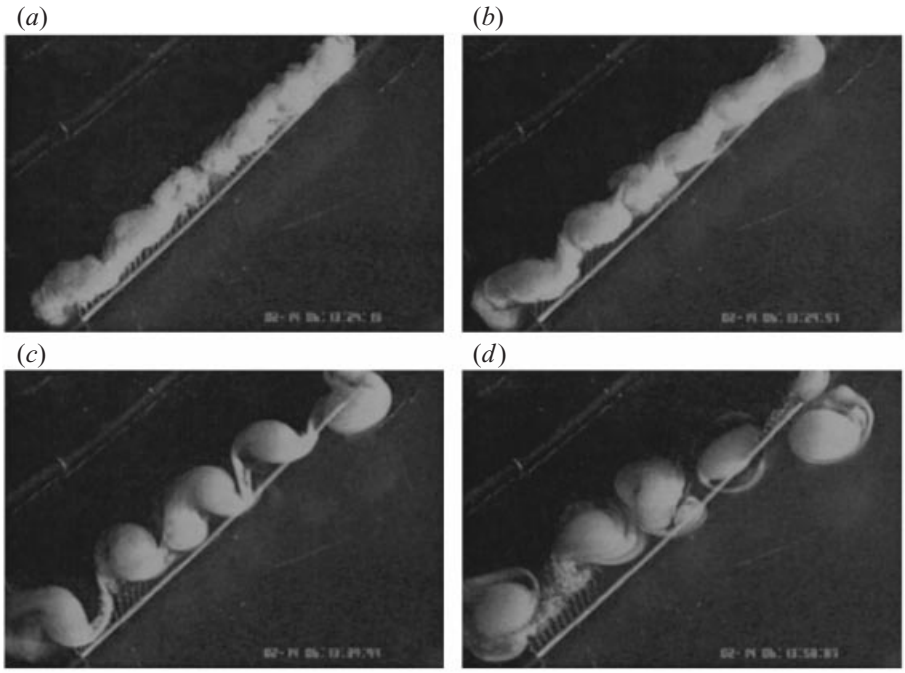

FIGURE 2. The instability of a line plume in a rotating stratified fluid. (*a*) $t = 7.3/f$: the turbulent plume begins to intrude at its level of neutral buoyancy, (*b*) $t = 13.6/f$: a strong horizontal shear develops across the neutral cloud, (*c*) $t = 14.5/f$: the neutral cloud breaks into six lenticular vortices, two of which merge, leaving (*d*) $t = 23/f$: five stable anticyclonic vortices. Note that the last three images were captured after the termination of the source: the weak tendrils evident therein are not the fully developed plume, but result from buoyant fluid leaking from the source. The plume merger is not evident in the first image owing to the oblique perspective.

the neutral cloud. Concurrently, entrainment into the plume generates a cyclonic flow beneath the neutral cloud, giving rise to a vertical shear across the base of the neutral cloud. The combined influence of the horizontal and vertical shears leads to instability of the neutral cloud, and to the formation of six lenticular anticyclonic vortices. A similar progression is captured in figure 3, which illustrates the emergence of four lenticular vortices as viewed from above. Figure 4 illustrates final states characterized by two, three, four and six vortices.

In a geostrophically balanced vortex, the radial pressure force is balanced by the Coriolis force associated with the anticyclonic swirling motion within the vortex, so that

$$fv_sR \sim N^2h^2, \tag{3.2}$$

where v_s is the magnitude of the swirling velocity and h and R denote, respectively, the half-height and radius of the vortex. The conservation of angular momentum within the plume fluid requires that $v_s \sim fR$; consequently, the aspect ratio of a geostrophically balanced vortex R/h is proportional to N/f. Figure 5 illustrates the dependence of the aspect ratio on N/f for the vortices observed in our experiments. Over the parameter range considered, the vortices took both prolate ($h/R > 1$) and oblate ($h/R < 1$) shapes. For all of the vortices observed in our experimental study,

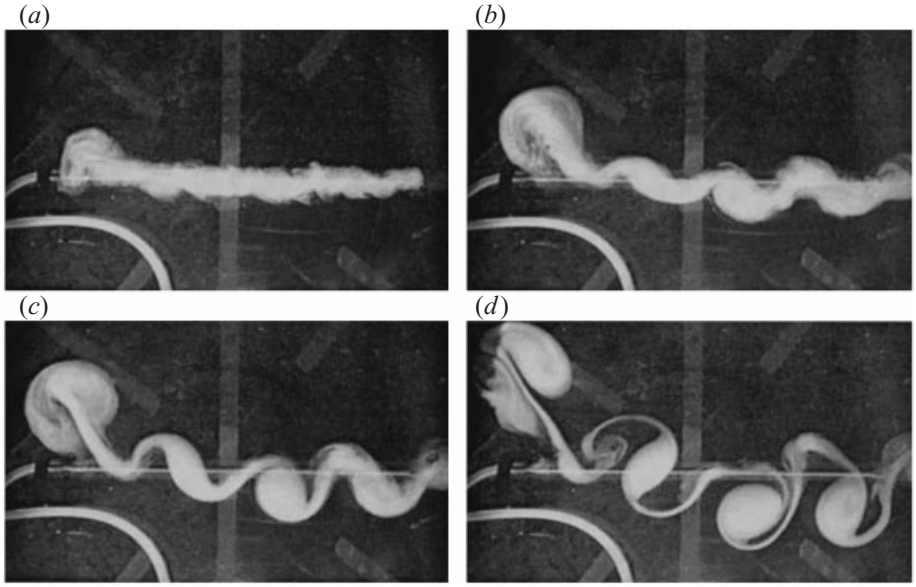

FIGURE 3. The instability of a line plume in a rotating stratified fluid, as viewed from above. (*a*) The plume reaches its level of neutral buoyancy. Its spread is resisted by the Coriolis force, which generates a strong shear across the neutral cloud. (*b*) The neutral cloud begins to go unstable. The plume source is turned off. (*c*) The neutral cloud wraps into four distinct anticyclonic vortices. (*d*) The persistence of four coherent vortical structures.

the Prandtl ratio was given by

$$P = \frac{Nh}{fR} = 0.47 \pm 0.12. \tag{3.3}$$

This value is comparable to those reported by Hedstrom & Armi (1988) who found $0.4 < P < 0.5$ in their study of single vortices generated by the release of fluid at its level of neutral buoyancy, but is slightly smaller than that reported by Helfrich & Battisti (1991) who found $0.5 < P < 0.8$ in their study of the neutral clouds above point plumes. It is important to note that the Prandtl ratio of a vortex in a rotating fluid will decrease with time as the vortex spins down through the influence of viscosity on a timescale $\tau \sim h/(f\nu)^{1/2}$. The measurements reported in figure 5 were made between ten and twenty rotation periods after the establishment of the vortices. The vortices were typically long-lived and stable, but did occasionally interact and merge directly after formation, as in the case illustrated in figure 2.

We proceed by presenting a simple scaling argument which indicates the dependence of the number of vortices on the governing parameters. The volume per unit length in the neutral cloud at the termination of the source is given by $Q(Z_n)\, t_s$. The instability transforms this volume into n lenticular vortices with half-height h and radius R. Continuity thus requires that

$$R\, h \;\sim\; Q(Z_n)\, t_s. \tag{3.4}$$

Using (3.1) for $Q(Z_n)$ and $h \sim Rf/N$, we obtain from (3.4) the characteristic radius of the vortices generated by the plume instability:

$$R \;\sim\; \frac{B^{1/3} t_s^{1/2}}{f^{1/2}}. \tag{3.5}$$

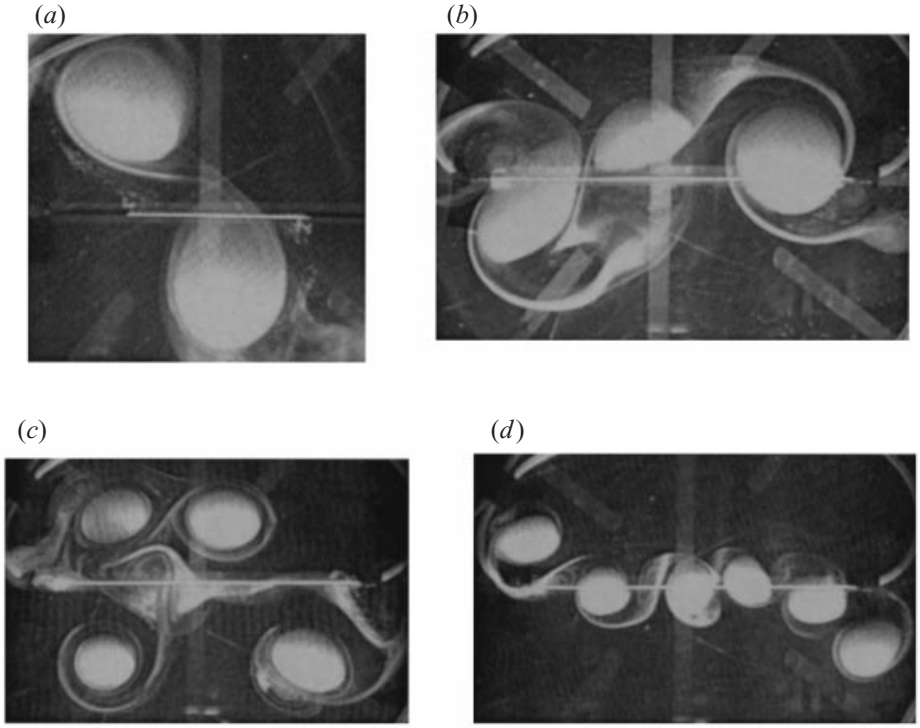

FIGURE 4. The stable vortex structures emerging from the instability of a line plume in a rotating stratified fluid. In (*a*) $N = 0.82$ s^{-1}, $B = 3.1$ cm^3 s^{-3}, $f = 0.4$ s^{-1}, $t_s = 30$s and $L = 21$ cm. In the other experiments, $N = 0.82$ s^{-1}, $B = 4.6$ cm^3 s^{-3}, and $L = 44$ cm, while f and t_s took the respective values of (*b*) 0.6 s^{-1} and 40 s, (*c*) 1.0 s^{-1} and 30 s, and (*d*) 1.5 s^{-1} and 25 s.

The number of such vortices is thus given by $n \sim L/R$, or

$$n = C_1 \frac{Lf^{1/2}}{t_s^{1/2} B^{1/3}}, \tag{3.6}$$

where C_1 is a constant of proportionality to be determined experimentally. This simple scaling indicates that the number of vortices is independent of the ambient stratification, but depends explicitly on the rate of rotation as well as the plume source conditions.

Figure 6 indicates the observed dependence of the number of vortices, n, on the governing parameters. The experiments validate the scaling (3.6), and indicate that $C_1 = 0.65 \pm 0.1$. It is noteworthy that situations arise where vortices of unequal size emerge: an integer number of vortices of radius $R = (0.77 \pm 0.12)B^{1/3}t_s^{1/2}/f^{1/2}$ emerge, in addition to a single vortex of approximately half the size. Such cases are represented by half-integer values of n in figure 6. the fact that n assumes only integer or half-integer values makes the experimental agreement with (3.6) all the more striking.

It is important to note that we have focused our study on the case of a finite release of fluid. In this case, the neutral cloud remains coherent until the source is terminated, at which stage it breaks into a train of eddies. By conservation of volume, the size of the eddies then depends explicitly on the duration of the source. Typically, the source was terminated soon after a well-defined wavelength became evident on the neutral

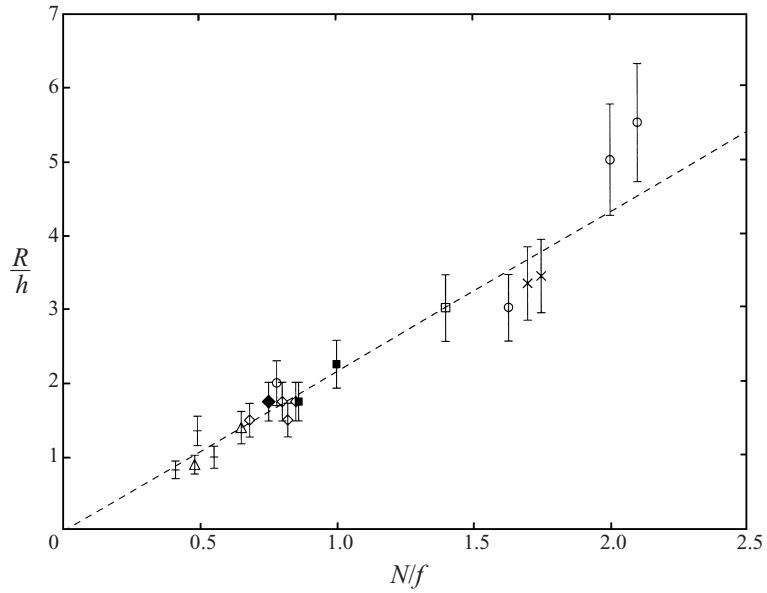

FIGURE 5. The observed dependence of the aspect ratio, R/h, of the lenses formed from the instability of a line plume on N/f. The dashed line represents a constant Prandtl ratio: $Nh/fR = 0.47$. The symbols $\times, \circ, \square, \diamond, \triangle, +$ indicate the number of vortices emerging from the instability of the neutral cloud, respectively, one to six, while the filled symbols correspond to the associated half-integer values.

cloud. However, for longer releases, there was an observable increase in the preferred wavelength of instability of the growing neutral cloud: the flow cascades to larger scales as the source persists. Consequently, one may identify a number of instability times at which progressively larger waveforms emerge on the neutral cloud.

In table 2 we list the time t_w from the initiation of plume discharge to the development of the final wavelength of instability of the neutral cloud (that corresponding to the final number of emerging vortices). While the reported values of t_w are subject to considerable error (± 3 s), they do suggest that t_w decreases with increasing rotation rate. While typically $t_w \sim t_s$, situations do arise where t_w is slightly less than t_s: the final wavelength is achieved before the termination of the source. This phenomenon results from the fact that there is some finite range of source times over which the same number of vortices will emerge.

We also performed a number of experiments in which the line plume release was continuous. In this case, the neutral cloud grows, and the waves on the neutral cloud cascade to larger scales until eventually instability of the neutral cloud leads to a complex flow characterized by cyclonic vortices spun-up by neighbouring anticyclones, and vortex dipoles which transport fluid away from the source region. As in the case of continuous release from a point plume (Helfrich & Battisti 1991), one expects the neutral cloud to grow until its depth is comparable to the intrusion height, $h_c \sim Z_n$, so that the resulting vortex radii, $R_c \sim Z_n N/f \sim B^{1/3}/f$, are independent of source time. Consequently, one expects the number of vortical structures emerging from each successive instability of the continuous line plume release to scale as $n \sim Lf/B^{1/3}$. At the onset of instability, continuity of plume fluid at the neutral height requires that $R_c h_c \sim Q(Z_n)t_i$. Using $R_c \sim h_c N/f$ and (3.1) for Z_n and $Q(Z_n)$ suggests an instability time of $t_i \sim 1/f$. This scaling for the timescale of instability of the neutral cloud above

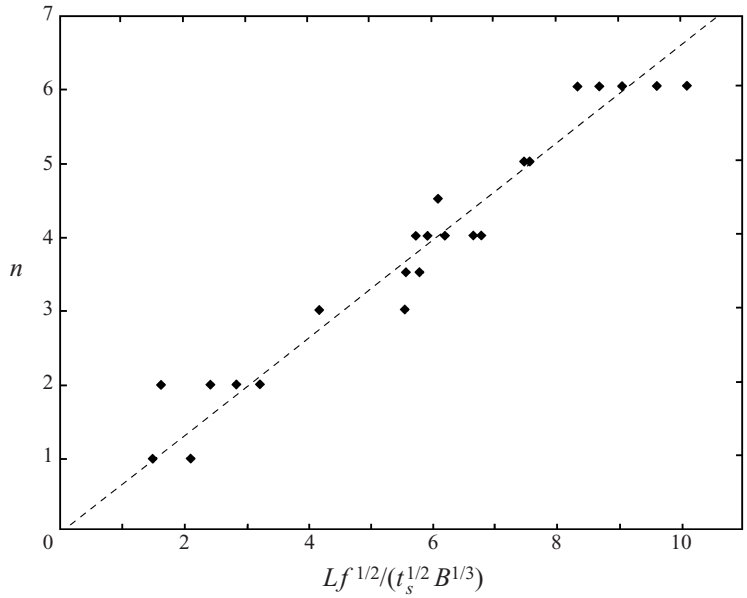

FIGURE 6. The observed dependence of the number of lenses, n, formed from a line plume impinging at its level of neutral buoyancy in a uniformly stratified ambient, on the non-dimensional group $Lf^{1/2}/(t_s^{1/2}B^{1/3})$. The dashed line represents $n = 0.65\ Lf^{1/2}/(t_s^{1/2}B^{1/3})$. The lenticular vortices were stable and long-lived.

a continuous line source differs from that above a point plume, for which $t_i \sim N/f^2$ (Helfrich & Speer 1995).

4. Homogeneous ambient

The flow variables of a two-dimensional line plume rising through a homogeneous non-rotating environment may be expressed in terms of the source buoyancy flux per unit length B and distance above the source z (Rouse *et al.* 1952). In particular, the volume flux Q, the mean buoyancy g', vertical velocity w and half-width b of the plume scale as

$$Q \sim \frac{B^{2/3}}{z}, \quad g' \sim B^{1/3}z, \quad w \sim B^{1/3}, \quad b \sim z. \tag{4.1}$$

We here consider the plume rising and impinging on a horizontal interface a distance H above the source. According to (4.1), the rise time in the absence of system rotation is given by $t_r \sim H/w \sim H/B^{1/3}$.

The ascent phase is influenced by the system rotation when $t_r > t_f$. The Taylor–Proudman Theorem requires that, in a homogeneous fluid in which flow is geostrophically balanced, there are no gradients in velocity in the direction parallel to the rotation axis (Taylor 1917). Consequently, we anticipate that the inherently z-dependent flow structure associated with a turbulent line plume will be strongly influenced by rotation. The influence of rotation on the plume dynamics may be characterized by the plume Rossby number, $Ro = w/(bf) \sim B^{1/3}f^{-1}z^{-1}$, which necessarily decreases with height above the source. The rotational plume lengthscale $L_f = B^{1/3}/f$ corresponds to the height at which $Ro = 1$: for $z > L_f$, the plume dynamics is dominated by rotation. Fernando & Ching (1993) have investigated a line plume advancing in a

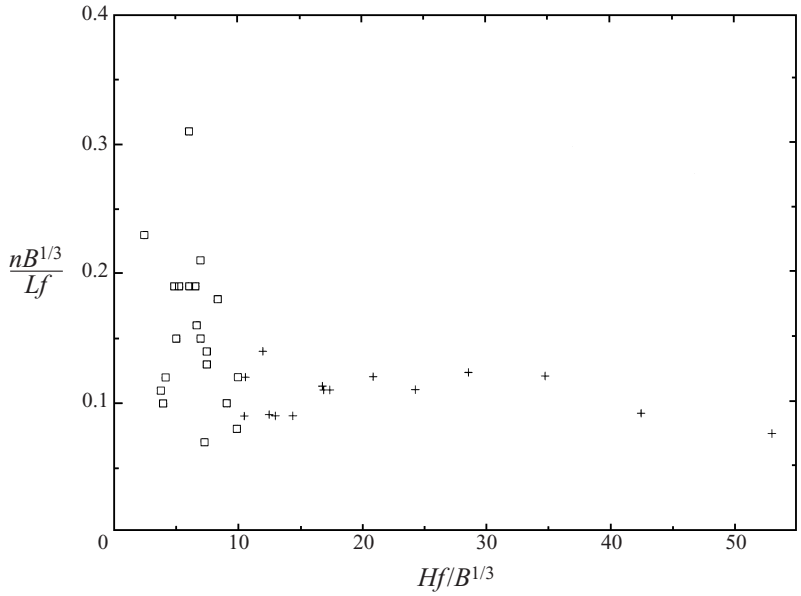

FIGURE 7. The observed dependence of the number of vortical structures emerging from a line plume discharging into a homogeneous ambient of depth H. Note the transition in scaling behaviour at $H_c \sim 10B^{1/3}/f$, which indicates the height at which rotation begins to influence the plume dynamics. The $\square$ correspond to the shallow layer ($H < H_c$) results reported in figure 10, and $+$ to the deep layer ($H > H_c$) results reported in figure 12.

rotating fluid, and found that the depth, z, of the plume cap initially increases as $z = 1.2\ B^{1/3}t$ in accordance with (4.1). However, after advancing a distance $6.4B^{1/3}/f$, the plume ascent becomes influenced by rotation. Specifically, the entrainment into the plume is suppressed, and the flow becomes strongly three-dimensional. The experiments of Fernando & Ching (1993) and the numerical study of Lavelle & Smith (1996) indicate that sinking line plumes are characterized by cyclonic flow in the region of entrainment above the plume head, and anticyclonic motion within the expanding head.

The form taken by the coherent structures emerging from the plume instability in the homogeneous ambient depends critically on the relative magnitudes of the layer depth H and the plume rotational lengthscale L_f. Figure 7 illustrates the dependence of the number of vortices observed on H/L_f, which suggests that the data cannot be collapsed with a simple scaling, and that a transition occurs at approximately $H \sim 10L_f$. Note that the results of Fernando & Ching (1993) indicate that this transition height corresponds roughly to that at which rotation begins to influence the plume ascent.

4.1. *Rise phase uninfluenced by rotation: $H < 10L_f$*

For the shallow layer, $H < 10L_f$, we expect the ascent phase of the plume motion to be unaffected by rotation, in which case the scaling (4.1) applies. The plume impinges on the free surface and spreads until rotation prompts an instability which is analogous to that in the uniformly stratified case: the surface current breaks up into a series of anticyclonic surface eddies. The breakup of a surface gravity current into five anticyclonic surface eddies, and the subsequent interaction and destruction of the eddies is illustrated in figure 8. Figure 9 illustrates the pair of surface eddies formed

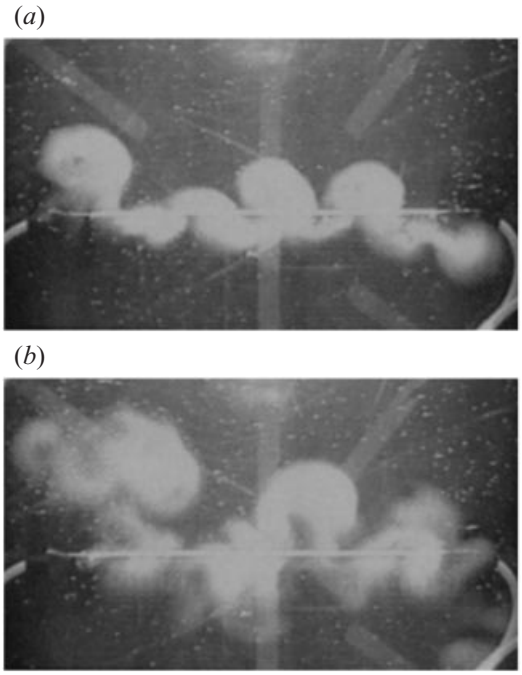

FIGURE 8. The evolution of surface eddies created by the impingement of a line plume on a free surface in a shallow layer: $f = 2\,\mathrm{s}^{-1}$, $L = 44$ cm, $B = 3.7\,\mathrm{cm}^3\,\mathrm{s}^{-3}$, $H = 10$ cm, $Hf/B^{1/3} = 13.0$, $t_s = 30$ s. (*a*) $t = 21/f$: the emergence of five surface eddies. (*b*) $t = 48/f$: the complex flow field resulting from their subsequent interaction.

by the impingement of a line plume on the free surface, as revealed through tracking particles suspended on the free surface. The resulting surface eddies were not as stable as their counterparts in the stratified ambient, and were more prone to destruction through mutual interaction. Moreover, it is worth noting that the instability of the surface current was typically not as regular as that in the stratified system, possibly owing to the disruptive influence of surfactants and Ekman layers on the free surface. The experimental data for this series of experiments are given in table 3.

We can deduce the scale of the resulting surface vortices by again coupling the dynamics of turbulent line plumes and geostrophic vortices. Continuity requires that volume per unit length of the surface current at the onset of instability is given by

$$R\,h \;\sim\; Q(H)\,t_s. \tag{4.2}$$

When the surface current goes unstable, it breaks into a series of geostrophic vortices of depth h and radius $R \sim (g'h)^{1/2}/f$. Using (4.1) for g', one may thus express h as

$$h \sim \frac{R^2 f^2 H}{B^{2/3}}. \tag{4.3}$$

Substituting (4.3) and $Q(H) \sim B^{1/3}H$ into (4.2) yields the radius characterizing the emerging vortices:

$$R \;\sim\; \frac{B^{1/3} t_s^{1/3}}{f^{2/3}}. \tag{4.4}$$

Consequently, the number of vortices resulting from the instability of the surface

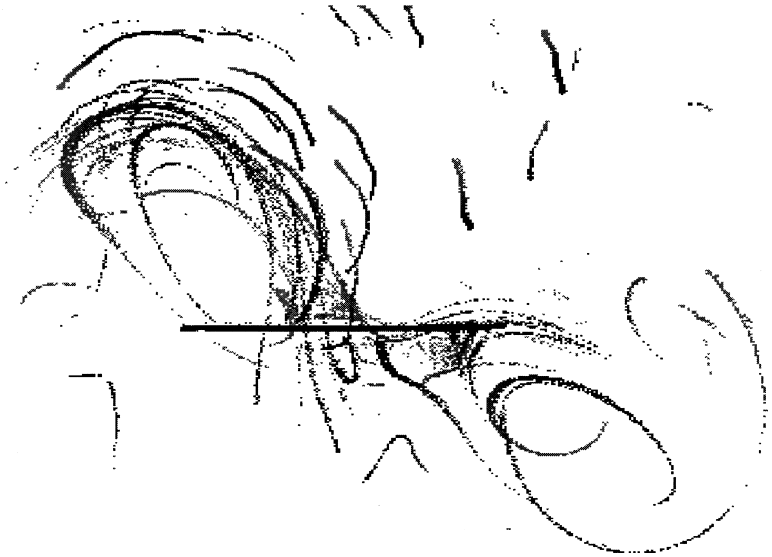

FIGURE 9. A pair of anticyclonic surface eddies formed by a line plume impinging on a free surface in a shallow layer, as revealed through tracking particles on the free surface: $f = 1.0\ \mathrm{s}^{-1}$, $L = 20\,\mathrm{cm}$, $B = 6.81\,\mathrm{cm}^3\mathrm{s}^{-3}$, $H = 11\,\mathrm{cm}$, $Hf/B^{1/3} = 5.3$, $t_s = 20\,\mathrm{s}$.

Expt	H (cm)	f (s^{-1})	L (cm)	QL ($\mathrm{cm}^2\ \mathrm{s}^{-1}$)	B ($\mathrm{cm}^3\ \mathrm{s}^{-3}$)	t_s (s)	H/L_f	n
4-1	10.0	2.0	44.0	4.5	3.7	20	13.0	5
4-2	34.0	2.0	44.0	4.5	4.0	35	42.5	5
4-3	27.0	1.0	44.0	4.5	4.0	15	16.9	3
4-4	19.0	1.2	44.0	4.5	4.0	20	14.4	3–4
4-5	14.0	1.2	44.0	4.5	4.0	16	10.6	4–5
4-6	10.0	2.0	44.0	4.5	4.0	18	12.5	5
4-7	7.0	2.4	44.0	4.5	4.0	14	10.5	5–6
8-2	33.0	1.1	40.0	4.6	1.13	33	34.8	5–7
8-5	28.0	1.0	20.0	4.6	4.6	20	16.8	1–2
8-7	27.0	1.5	20.0	4.6	4.6	30	24.3	2
9-1	12.5	2.0	20.0	2.0	2.94	15	17.4	3
9-2	12.5	2.4	20.0	2.0	2.94	23	20.9	4
9-5	12.5	1.5	20.0	2.0	2.94	25	12.0	3
10-6	8.0	2.0	40.0	4.5	3.85	10	10.0	6
10-7	8.0	2.0	40.0	4.5	3.85	6	10.0	6
15-1	35.0	1.2	40.0	4.63	3.18	35	28.6	4
15-2	40.0	2.2	40.0	4.63	4.53	60	53.0	4

TABLE 3. Experimental data for line plumes rising through a rotating homogeneous environment for $H/L_f \geqslant 10$. The plume ascent is influenced by the ambient rotation, and a series of n unstable columnar structures emerge before surfacing.

current is given by $n \sim L/R$, or

$$n = C_2 \frac{L f^{2/3}}{B^{1/3} t_s^{1/3}}, \tag{4.5}$$

where C_2 is a coefficient to be determined experimentally. We note that in this limit of $H < 10L_f$, the number of vortices emerging is independent of the distance H

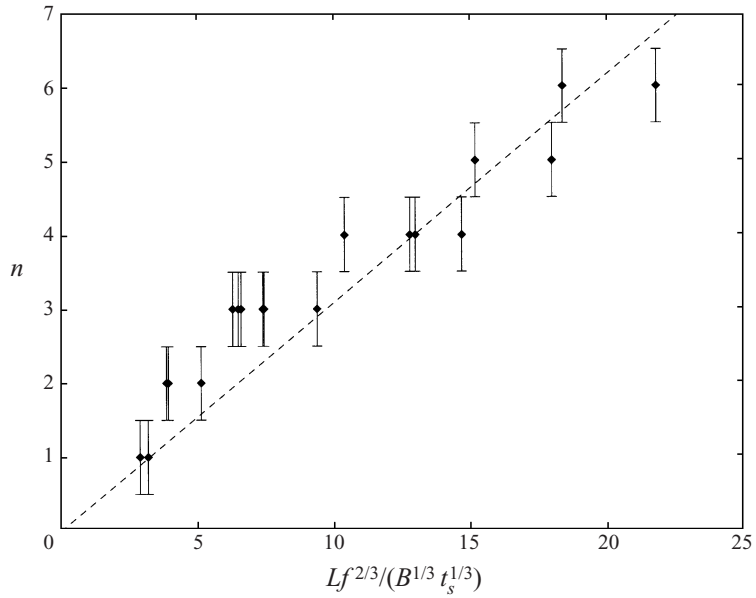

FIGURE 10. The observed dependence of the number of surface eddies, n, formed from the instability of a line plume impinging on a free surface a distance $H < 10B^{1/3}f^{-1}$ from the source in a homogeneous environment. The dashed line represents $n = 0.31\ Lf^{2/3}/(Bt_s)^{1/3}$.

between the source and the interface. Figure 10 indicates the dependence of the number of surface eddies, formed from the instability of the surface gravity current, on the source conditions. The data strongly support the validity of the scaling result (4.5) and indicate that $C_2 = 0.31 \pm 0.06$. Note again that the number of vortices is an integer, which makes the agreement even more striking. The origin of the errors reported in n is discussed in § 4.3.

We note again the important distinction between the cases of finite and continuous release. The physical picture given above describes the case of a finite release, for which n depends explicitly on the source time t_s. If the release were instead continuous, then one would expect the neutral cloud to grow until its thickness becomes comparable to the layer depth H, so that the radii of the emerging vortices would scale as $R \sim (g'(H)H)^{1/2}/f \sim B^{1/3}/f$. One would thus expect the number $n \sim L/R \sim Lf/B^{1/3}$ of vortices emerging from the continuous line source release to be independent of source time. That this continuous-release scaling does not adequately describe our data is made clear in figure 7: if it did, then all of the shallow layer data, denoted by □, would lie on a horizontal line.

4.2. *Rise phase influenced by rotation: $H > 10L_f$*

The least-stable vortical structures which emerged from the instability of a line plume were those observed in the case of the deep layer, $H > 10L_f$. In this case, the plume broke into a series of slowly ascending tall columnar structures. Although the resulting Taylor column structures were typically destroyed by mutual interaction before reaching the free surface, it was possible to identify a dominant wavelength of instability of the rising line plume, and so too the number of Taylor column structures at the onset of instability. The experimental data are given in table 4. Figure 11 illustrates the development of Taylor column structures above a rising line plume, and their subsequent collapse through mutual interaction.

Expt	H (cm)	f (s^{-1})	L (cm)	QL (cm^2 s^{-1})	B (cm^3 s^{-3})	t_s (s)	H/L_f	n
4-8	5.8	2.0	44.0	4.5	4.0	26	7.3	4
4-9	6.0	1.0	44.0	4.5	4.0	30	3.8	3
5-1	21.0	0.4	44.0	4.5	5.0	20	4.9	2
5-2	17.5	0.6	44.0	4.5	5.0	15	6.1	2–3
5-3	15.0	0.8	44.0	4.5	5.0	13	7.0	3
5-4	11.5	1.0	44.0	4.5	5.0	15	6.7	4
5-5	8.5	0.5	44.0	4.5	5.0	15	2.5	3
9-3	12.5	1.0	20.0	4.63	6.81	20	6.6	2
9-4	12.5	1.0	20.0	4.63	6.81	35	6.1	1
9-6	11.0	1.2	20.0	2.0	2.94	16	8.4	3
9-7	11.0	1.0	20.0	2.0	2.94	10	7.0	3
9-8	11.0	1.0	20.0	4.63	6.81	20	5.3	2
9-9	11.0	0.8	20.0	4.63	6.81	30	2.9	1
10-1	10.0	1.0	40.0	4.5	7.7	20	5.06	3
10-2	10.0	1.5	40.0	2.0	3.43	20	9.9	3
10-3	9.0	2.0	40.0	4.5	7.7	15	9.1	4
10-4	4.0	2.0	40.0	2.0	3.43	10	4.0	4
10-5	8.0	1.5	40.0	4.5	3.85	10	7.5	5
10-8	8.0	1.5	40.0	4.5	3.85	6	7.5	5

TABLE 4. Experimental data for line plumes rising through a rotating homogeneous environment for $H/L_f < 10$. Rotation does not influence the plume ascent, but causes the resulting surface current to break into n anticyclonic surface eddies.

For a deep layer, $H > 10L_f$, we expect the spread of a rising line plume to be suppressed at a distance comparable to $10L_f$ from the source, above which the plume breaks into a series of anticyclonic columnar structures of characteristic radius L_f. While detailed measurements of the plume velocity field were not taken, observations suggested that, as in the case considered by Helfrich (1994) of thermals released from a point source, rotation served here to suppress the lateral spread of the plume, without dramatically altering its rate of ascent. The number of vortices shed from a turbulent line plume of length L is expected to scale as

$$n = C_3 \frac{L f}{B^{1/3}}. \tag{4.6}$$

Figure 12 illustrates the observed dependence of the number of Taylor columns emerging from the plume as a function of the source parameters and rotation rate. The data support the scaling result (4.6), and indicate that $C_3 = 0.11 \pm 0.015$. The substantial errors reported in n are again discussed in § 4.3. We note that this is the only case considered in which the radii of the emerging structures does not depend explicitly on the source time t_s. In this case, there was no cascade to larger scales as the source persisted, and the plume structure went unstable to the first pronounced wave-like disturbance. The instability of the line plume thus gives rise to a series of columns whose radius is prescribed uniquely by the source buoyancy flux and system rotation: the source time prescribes the total volume and so the vertical extent of the resulting columns, but not their radial extent at the onset of instability. Finally, we note that result (4.6) should also be valid for stratified ambients provided $f \gg N$.

It is noteworthy that the previous investigations of line plumes in rotating homogeneous fluids by Fernando & Ching (1993) and Lavelle & Smith (1996) were carried out in the parameter regime $L/L_f < 15$, for which (4.6) indicates that the number

(*a*)

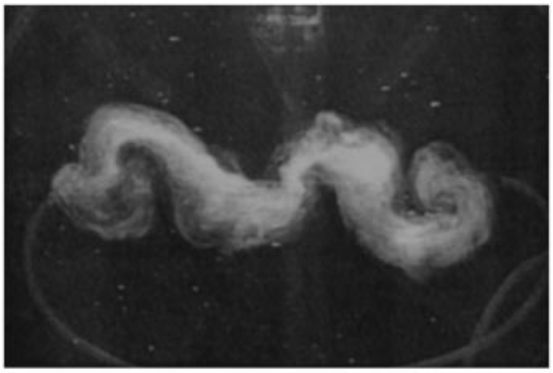

(*b*)

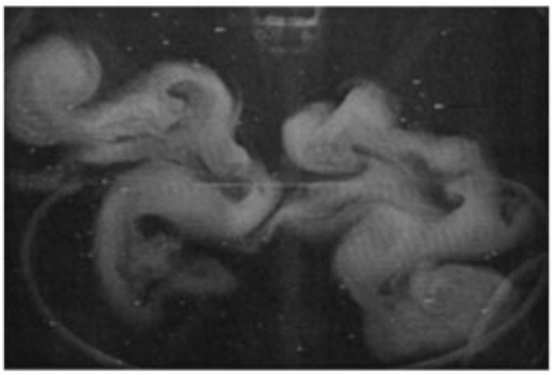

FIGURE 11. The evolution of Taylor columns generated by a line plume discharging into a deep homogeneous ambient: $f = 1.5\,\mathrm{s}^{-1}$, $B = 4.6\,\mathrm{cm}^3\mathrm{s}^{-3}$, $H = 27\,\mathrm{cm}$, $L = 20\,\mathrm{cm}$, $t_s = 30\,\mathrm{s}$, $Hf/B^{1/3} = 24.3$. (*a*) $t = 28/f$: the onset of instability of the line plume giving rise to Taylor column structures impinging on the free surface. (*b*) $t = 58/f$: the subsequent turbulent structure resulting from the interaction and collapse of the Taylor columns.

of emerging Taylor columns should be one or two. Presumably, this is why the rotationally induced break-up of a line plume into a number of discrete Taylor column structures has not previously been clearly identified.

4.3. *Discussion of errors*

The principal difficulty in the experiments was the maintenance of a uniform line source. While attempts were made to minimize the variations along its length, they could not be eliminated entirely, and the plume fluid generally emerged from either end of the source before reaching its centre. Such non-uniformity could act in certain circumstances to influence the preferred mode of instability. In particular, as suggested by figure 6, instabilities characterized by an even number of modes were generally preferred. Also, in the case of the experiments in the homogeneous ambient, particularly those in the deep layer ($H > 10B^{1/3}/f$) where the columns were particularly unstable, it was not always possible to identify unequivocally the number of modes forming. This difficulty accounts for the large errors in n reported in figure 12. Similar difficulties arose, but were less pronounced, in the shallow layer experiments and account for the errors in n reported in figure 10. In the stratified ambient, no such difficulties arose.

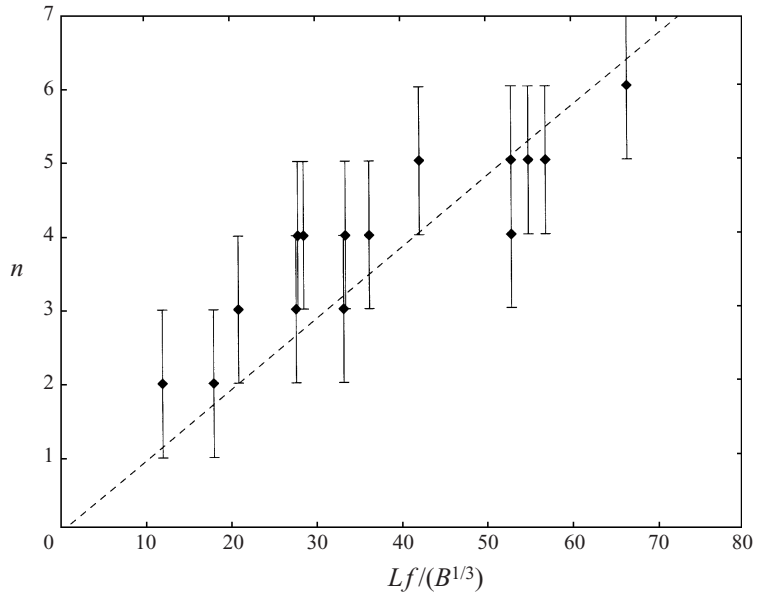

FIGURE 12. The observed dependence of the number of columnar vortices, n, formed from the instability of a line plume in a homogeneous environment, on the non-dimensional group $Lf/B^{1/3}$ for $H > 10\ B^{1/3}/f$. The dashed line represents $n = 0.095\ Lf/B^{1/3}$. The columnar vortices were unstable, and their coherence was rapidly destroyed by mutual interaction.

Another source of error was the inevitable deviation of the flow in the neighbourhood of the source from that predicted to exist from standard plume theory. The flow above any real source may be subdivided into three regions: the zone of flow establishment (adjoining the source), wherein the flow is not fully turbulent and is influenced by the details of the source geometry; the jet zone, wherein the flow is dominated by the initial momentum of the source fluid; and the plume zone (furthest from the source), wherein the flow is buoyancy driven, and the plume scaling of Morton *et al.* (1956) applies. Our source consisted of a series of individual plumes spaced 0.5 cm apart, which merged into a line plume approximately 2 cm above the source. Experiments on line plumes indicate that the jet length is typically $1.4MB^{-2/3}$ where M is the source momentum flux per unit length (Linden & Simpson 1990), which for our experiments corresponds to a distance of no greater than 1 cm. We conclude that the observed flows adjusted to a pure plume-like state after rising approximately $L_a \sim 2$–3 cm above the source. In the experiments in the stratified ambient, it is the uncertainty in this adjustment length L_a which accounts for the considerable error reported in the coefficient of the neutral height $Z_n = (3.0 \pm 1.0)B^{1/3}/N$.

5. Oceanographic applications

5.1. *The generation of eddies by leads in the Arctic Ocean*

Wind stresses lead to mechanical failure of the polar ice caps, and so to the formation of leads which are typically 1–100 m wide and may extend several hundred kilometres in length. Brine is rejected from the ice as it refreezes on a timescale of a week, leading to a negatively buoyant line plume sinking through the ocean depths (Morison *et al.* 1992). Typically, the plume will impinge on the pycnocline at the base of the mixed

layer whose depth varies seasonally between 30 and 50 m. On the basis of our study of line plumes impinging on an interface, we proceed by making inferences concerning the generation of oceanic eddies by polar leads.

Choosing values describing the impingement of oceanic leads on the pycnocline, $H = 50\,\mathrm{m}$, $t_s = 1$ week, $f = 1.4 \times 10^{-4}\,\mathrm{s}^{-1}$ and $B = 544\,\mathrm{cm}^3\,\mathrm{s}^{-3}$ (Morison *et al.* 1992) indicates that the descent time $t_r \sim H/B^{1/3}$ is much shorter than the source time. Moreover, $H < 10\ B^{1/3}/f = 5.8\,\mathrm{km}$, so that the descent phase will be unaffected by rotation, and our physical picture described in § 4.1 will apply. In the absence of substantial ambient currents, the plume fluid will impinge on the pycnocline, and spread for several days until it develops an instability and breaks into a chain of anticyclonic eddies. The number of such eddies is given by (4.5) where L now represents the lead length. Choosing the aforementioned lead source conditions indicates that the vortices formed by lead-induced thermohaline convection would have a characteristic diameter of 10 km. This corresponds roughly to the scale of the anticyclonic lenticular vortices prevalent at the base of the mixed layer in the Arctic Ocean (Manley & Hunkins 1985). A more detailed discussion of the relevance of this study to the problem of vortex generation by lead-induced thermohaline convection will be the subject of a forthcoming paper.

5.2. *Hydrothermal venting*

Observations have recently been made of lenticular clouds of hydrothermal fluid of characteristic depth 500 m and diameter 15 km located 1 km above mid-ocean ridge systems (Baker 1995). The origin of these 'megaplumes' is unclear; however, it is generally thought to be associated with a cataclysmic event increasing the permeability of the shallow crust and so facilitating the rapid outflow of a substantial volume of hydrothermal fluid (Cann & Strens 1989; Baker *et al.* 1989). The work presented here indicates that, if such an event created a sufficiently long crack in the seafloor, then one would anticipate the simultaneous release of several megaplumes. Moreover, on the basis of the simple physical picture presented herein, it is possible to make inferences concerning the source conditions from the geometry of the megaplumes (Woods & Bush 1999).

The formation of coherent vortical structures has also been observed by Helfrich & Speer (1995), who were concerned with the influence of tides on the dispersal of hydrothermal effluent from individual black smoker plumes on the seafloor. The influence of the tides was modelled experimentally by moving a point plume source along a line in a temporally periodic fashion. The resulting vortices observed may be understood in the context of the present work: the tides act to make the point source of buoyancy flux B_0 behave as a line source with buoyancy flux $B = B_0/L$ per unit length, where L is twice the amplitude of the tidal displacement. Assuming that the cross-flow is weak, so that the entrainment is not significantly affected by the plume tilting, we expect the number of vortices to emerge in a stratified ambient to be given by $n \sim Lf/B^{1/3}$ for the case of a continuous release, or equation (3.6) for a release of finite duration.

6. Conclusions

Through coupling the dynamics of turbulent plumes and geostrophic eddies, we have developed a model describing the generation of vortical structures from extended sources in rotating systems. The predicted scalings for finite releases of buoyant fluid have been validated by a comprehensive experimental study of line plumes in rotating

systems, which allow us to make quantitative predictions concerning the size of vortical structures generated from line plume releases in rotating fluids. In the previous studies of related instabilities in axisymmetric geometries, fluid systems have been considered in which a lengthscale arises naturally in the problem, specifically the layer depth. On the basis of this length, one may define a Rossby deformation radius which sets the scale of the instability. In our problem, we have defined this critical lengthscale in terms of the plume source conditions and demonstrated that, for $t_s < t_i$, it depends explicitly on the duration of the source.

The instability of the neutral cloud in the stratified environment, and of the surface current in the shallow homogeneous layer, is qualitatively similar to that examined by Griffiths *et al.* (1982). They released buoyant fluid of reduced gravity g' from a cylindrical annulus of depth H_0 and width W_0 at the surface of a homogeneous rotating ambient, and examined the instability of the two fronts on the inner and outer surfaces of the spreading current. They demonstrated that the nature of the instability depends on the relative magnitudes of W_0 and the Rossby radius of deformation $R = (g'H_0)^{1/2}/f$. For wide currents, $W_0/R > 1$, the inner and outer fronts behave independently, giving rise to a complex disordered flow, characterized by cyclonic, anticyclonic and dipolar vortices, which was qualitatively similar to that observed in our experiments for which $t_s \gg t_i$. For narrow currents, $W_0/R < 1$, the instabilities of the inner and outer fronts are coupled, and the current breaks into a chain of anticyclonic vortices as in our experiments when $t_s < t_i$. This form of flow was predicted by their linear analysis of the instability of an initially two-dimensional geostrophic current spreading in an infinitely deep homogeneous rotating environment, which indicated a most unstable mode characterized by a wavelength $1.25R$ and a growth rate $8/f$. Griffiths *et al.* (1982) identified the possibility of both meandering and varicose modes of instability, in which the sinusoidal disturbances on the neighbouring fronts are, respectively, in phase and out of phase. In our study of finite-duration releases, the instability of the neutral cloud in the stratified fluid was characterized by a varicose mode (figures 2 and 3), that of the plume in the deep homogeneous layer was meandering (figure 11), and that of the surface current in the shallow homogeneous layer was mixed. A theoretical treatment of the instabilities examined in our experimental study would entail considering the evolution of an expanding neutral cloud or surface current in an ambient of finite depth, in addition to the influence of the vertical shear at the base of the neutral cloud generated by the entrainment into the plume.

Table 5 summarizes the principal results of this paper for the radius of the coherent structures emerging from discrete releases of buoyant fluid from line sources in a rotating ambient. The number of such structures formed from a line source of length L is given by $n = L/(2R)$. For the case of a finite-duration discharge into a stratified ambient, the coherent structures take the form of long-lived lenticular anticyclonic vortices with a constant Prandtl ratio $P = 0.47 \pm 0.12$. For a finite-duration discharge into a homogeneous ambient, the physical picture differs according to the layer depth. For $H > 10\ B^{1/3}/f$, the ascent phase is influenced by rotation, and the line plume breaks into a series of anticyclonic columnar vortices. These Taylor column structures are unstable, and typically interact and collapse before surfacing. For $H < 10\ B^{1/3}/f$, rotation only becomes important during the spreading phase of the surface gravity current, which breaks into a series of anticyclonic surface eddies.

Table 5 also includes the scaling appropriate for describing the related problem of line thermals, which arise when the source time is much less than the rise time, $t_s \ll t_r$, so that the release may be considered as instantaneous. The scaling analysis

	Stratified ambient	Homogeneous ambient ($H < 10\ B^{1/3}/f$)	Homogeneous ambient ($H > 10\ B^{1/3}/f$)
Structures	stable anticyclonic lenticular vortices	stable anticyclonic surface eddies	unstable anticyclonic columnar vortices
Finite plume release	$(0.77 \pm 0.1)\ \dfrac{B^{1/3} t_s^{1/2}}{f^{1/2}}$	$(1.6 \pm 0.2)\ \dfrac{B^{1/3} t_s^{1/3}}{f^{2/3}}$	$(5.3 \pm 1.0)\ \dfrac{B^{1/3}}{f}$
Thermal	$\sim \dfrac{F^{1/3}}{f^{1/2} N^{1/6}}$	$\sim \dfrac{F^{1/3}}{f^{2/3}}$	$\sim \dfrac{F^{1/3}}{f^{2/3}}$

TABLE 5. Summary of results for the radius of vortices emerging from a discrete release of buoyant fluid from a line source in a rotating ambient. For the case of a line plume discharging into a homogeneous ambient and impinging on an interface, we report results for the cases where the rise height H is both larger and smaller than the rotational lengthscale $10\ B^{1/3}/f$. The related scalings for the instantaneous release of a line thermal (see the Appendix) are also included.

leading to these results is similar to that presented in § 3 and § 4, and is included for completeness in the Appendix. While a number of experiments were carried out in order to investigate the thermal problem, difficulties associated with irregularity of the source precluded a thorough experimental investigation. Nevertheless, coherent vortical structures were observed, and we expect the physical picture described in Appendix A to be appropriate.

We have also discussed briefly the continuous release of buoyant fluid from a line source, in which the neutral cloud grows until its depth is comparable to the intrusion height. Thereafter, the neutral cloud goes unstable, resulting in a complex flow structure including dipolar and monopolar vortices which transport fluid away from the source. Scaling arguments suggest that the resulting structures will have characteristic radius $R \sim B^{1/3}/f$ in both the stratified and homogeneous ambients.

If the coherent vortical structures emerging from such mixing events were homogeneous, they would decay on a spin-down timescale (Hedstrom & Armi 1988), $\tau_s \sim h/(\Omega v)^{1/2}$, which is on the order of a year for an oceanic eddy of radius 5 km. Moreover, plume-generated vortices are typically internally stratified owing to the similarities between the establishment of the neutral cloud and the filling box process (Bormans & Turner 1990), and this internal stratification may render them even more stable and long-lived (Bormans 1992). We thus expect the anomalous temperature and chemical signatures of vortices formed by polar leads or hydrothermal venting to be maintained for a long time, and the presence of such structures to have a significant impact on oceanic mixing.

Although we have focused on the formation of vortical structures by line releases of buoyant fluid, we expect that a similar approach may be applied in describing other types of mixing events. For example, boundary mixing events in the ocean may give rise to gravity currents which propagate along continental slopes before intruding at their level of neutral buoyancy, and this process is one of the possible mechanisms responsible for the generation of the lenticular submesoscale vortices, termed 'meddies', from Mediterranean outflow (McWilliams 1985; Bormans & Turner 1990). By choosing an appropriate model for entrainment into gravity currents propagating along slopes, one may again link the source conditions to the number and scale of the resulting vortical structures. The phenomenon of eddy formation by a gravity current

descending on a slope in a rotating homogeneous fluid has recently been examined by Lane-Serff & Baines (1998).

Finally, we expect that the approach presented herein for describing the scale of coherent structures emerging from discrete line plume releases in rotating fluids has a broader relevance. For example, a similar model might be developed in order to describe the flow arising from turbulent mixing events in an electrically conducting fluid in the presence of a magnetic field. A more general description of the emergence of coherent flow structures from discrete mixing events and turbulent convection in the presence of constraints will be the subject of future work.

The authors gratefully acknowledge financial support through a NERC BRIDGE grant. The authors thank John Wettlaufer for a number of helpful discussions, and Paul Linden for providing a congenial work environment for J.W.M.B. in the DAMTP Fluids Laboratory.

Appendix. Line thermals

If the source time is considerably less than the ascent time, $t_s \ll t_r$, the release may be described as that of a line thermal of volume $V = Qt_s$ and buoyancy $F = g'V = Bt_s$ per unit length. If the ambient is stratified, then the rise height Z_n, the ascent time t_r, as well the volume per unit length $V(Z_n)$ at the intrusion height may all be expressed in terms of F and N through

$$Z_n \sim \frac{F^{1/3}}{N^{2/3}}, \quad t_r \sim \frac{1}{N}, \quad V(Z_n) \sim \frac{F^{2/3}}{N^{4/3}}. \tag{A 1}$$

The influence of rotation is thus negligible during the ascent phase provided $N \gg f$.

Continuity at the spreading level requires that

$$R\,h \sim V(Z_n). \tag{A 2}$$

Again noting that $h \sim Rf/N$ for geostrophically balanced vortices yields their characteristic radius

$$R \sim \frac{F^{1/3}}{f^{1/2}N^{1/6}}. \tag{A 3}$$

The number of anticyclonic lenticular vortices resulting from the instability of the neutral cloud is thus given by $n \sim L/R$, or

$$n \sim \frac{Lf^{1/2}N^{1/6}}{F^{1/3}}, \tag{A 4}$$

which in this case has a weak dependence on the degree of stratification.

When the ambient is homogeneous and the ascent phase is not influenced by the system rotation, the variables of the line thermal depend exclusively on F and the distance z above the source; in particular,

$$b \sim z, \quad w \sim F^{1/2}z^{-1/2}, \quad g' \sim Fz^{-2}, \quad V \sim z^2, \tag{A 5}$$

where b is the characteristic width of the thermal (Richards 1963). The thermal rises and expands through the homogeneous ambient until it reaches the free surface at $z = H$ after a time $t_r \sim H/w \sim H^{3/2}F^{-1/2}$.

The scaling (A 5) indicates that the Rossby number which characterizes the thermal

will vary with height above the source as

$$R_o = \frac{w}{fb} \sim \frac{F^{1/2}}{z^{3/2}f}. \tag{A 6}$$

Consequently, we expect the flow to be rotationally dominated after rising a distance

$$L_t \sim \frac{F^{1/3}}{f^{2/3}}. \tag{A 7}$$

When $H \gg L_t$, the ascent phase will be dominated by rotation, and the line thermal will break into a series of anticyclonic vortices of characteristic scale L_t; consequently, we expect that an instantaneous release of length L to produce

$$n \sim \frac{L\, f^{2/3}}{F^{1/3}} \tag{A 8}$$

discrete columnar vortices.

Rotation does not influence the ascent phase of the thermal provided $H \ll L_t$, in which case the thermal cloud spreads at the free surface before developing a rotationally induced instability. Conservation of volume in the spreading surface current requires that

$$R\, h \sim V(H). \tag{A 9}$$

As in §4.1, the height and radius of the resulting vortices are related through $h \sim R^2 f^2/g'$, and since the thermal intruding at the free surface has reduced buoyancy $g' \sim F/H^2$, we have

$$h \sim \frac{R^2 f^2 H^2}{F}. \tag{A 10}$$

Substituting h and $V(H) \sim H^2$ into (A 9) thus yields the radius characterizing the resulting vortices:

$$R \sim \frac{F^{1/3}}{f^{2/3}}. \tag{A 11}$$

The number of anticyclonic eddies emerging at the free surface will thus be $n \sim L/R$, or

$$n \sim \frac{L\, f^{2/3}}{F^{1/3}}, \tag{A 12}$$

which is again independent of H. We note that the scalings for the latter two cases are identical.

REFERENCES

Ayotte, B. A. & Fernando, H. J. S. 1994 The motion of a turbulent thermal in the presence of background rotation. *J. Atmos. Sci.* **51**, 1989–1994.

Baker, E. T. 1995 Characteristics of hydrothermal discharge following a magmatic intrusion. In *Hydrothermal Vents and Processes*. Geol. Soc. Spec. Pub. No. 87, pp. 65–76.

Baker, E., Lavelle, J., Feely, R., Massoth, G. & Walker, S. 1989 Episodic venting of hydrothermal fluids from the Juan de Fuca Ridge. *J. Geophys. Res.* **94**, 9237–9250.

Bormans, M. 1992 An experimental study on the formation and survival of stratified subsurface eddies. *J. Geophys. Res.* **97** (C12), 20155–20167.

Bormans, M. & Turner, J. S. 1990 The formation of the doubly stable stratification in the Mediterranean Outflow. *Deep-Sea Res.* **37**, 1697–1712.

Boubnov, B. M. & Heijst, G. J. F. van 1994 Experiments on convection from a horizontal plate with and without background rotation. *Exps. Fluids* **16**, 155–164.

Bush, J. W. M. & Woods, A. W. 1998 Experiments on buoyant plumes in a rotating channel. *Geophys. Astrophys. Fluid Dyn.* **89**, 1–22.

Cann, J. & Strens, M. 1989 Modeling periodic megaplume emission by black smoker systems. *J. Geophys. Res.* **94**, 12227–12237.

Ching, C. Y., Fernando, H. J. S. & Noh, Y. 1993 Interaction of a negatively buoyant line plume with a density interface. *Dyn. Atmos. Oceans* **19**, 367–388.

Dalziel, S. B. 1992 Decay of rotating turbulence: some particle tracking experiments. *Appl. Sci. Res.* **49**, 217–244.

Elrick, J. R. 1979 Interaction between a discrete downdraft and a rotating environment. *J. Atmos. Sci.* **36**, 306–312.

Fernando, H. J. S., Chen, R.-R. & Ayotte, B. A. 1998 Development of a point plume in the presence of background rotation. *Phys. Fluids* **10**, 2369–2383.

Fernando, H. J. S., Chen, R.-R. & Boyer, D. L. 1991 Effects of rotation on convective turbulence. *J. Fluid Mech.* **228**, 513–547.

Fernando, H. J. S. & Ching, C. Y. 1993 Effects of backgound rotation on turbulent line plumes. *J. Phys. Oceanogr.* **23**, 2125–2129.

Griffiths, R. W., Killworth, P. D. & Stern, M. E. 1982. Ageostrophic instability of ocean currents. *J. Fluid Mech.* **117**, 343–377.

Griffiths, R. W. & Linden, P. F. 1981*a* The stability of vortices in a rotating, stratified fluid. *J. Fluid Mech.* **105**, 283–316.

Griffiths, R. W. & Linden, P. F. 1981*b* The stability of buoyancy-driven coastal currents. *Dyn. Atmos. Oceans* **5**, 281–306.

Griffiths, R. W. & Linden, P. F. 1981*c* Laboratory experiments on fronts. *Geophys. Astrophys. Fluid Dyn.* **19**, 159–187.

Hedstrom, K. & Armi, F. 1988 An experimental study of homogeneous lenses in a stratified rotating fluid. *J. Fluid Mech.* **191**, 535–556.

Helfrich, K. R. 1994 Thermals with background rotation and stratification. *J. Fluid Mech.* **259**, 265–280.

Helfrich, K. R. & Battisti, T. M. 1991 Experiments on baroclinic vortex shedding from hydrothermal plumes. *J. Geophys. Res.* **96**, 12511–12518.

Helfrich, K. R. & Speer, K. G. 1995 Oceanic hydrothermal circulation: mesoscale and basin-scale flow. In *Seafloor Hydrothermal Systems: Physical, Chemical, Biological and Geological Interactions*. Geophysical Monograph 91, AGU.

Ivey, G. N. 1987 Boundary mixing in a rotating stratified fluid. *J. Fluid Mech.* **183**, 25–44.

Johari, H. 1992 Mixing in thermals with and without buoyancy reversal. *J. Atmos. Sci.* **49**, 1412–1426.

Julien, K., Legg, S., McWilliams, J. & Werne, J. 1996 Rapidly rotating turbulent Rayleigh–Benard convection. *J. Fluid Mech.* **322**, 243–273.

Lane-Serff, G. F. & Baines, P. G. 1998 Eddy formation by dense flows on slopes in a rotating fluid. *J. Fluid Mech.* **363**, 229–252.

Lavelle, J. W. & Smith, D. C. 1996 Effects of rotation on convective plumes from line segment sources. *J. Phys. Oceanogr.* **26**, 863–872.

Linden, P. F. & Simpson, J. E. 1990 Continuous two-dimensional releases from an elevated source. *J. Loss Prev. Process Ind.* **3**, 82–87.

List, E. J. 1982 Turbulent jets and plumes. *Ann. Rev. Fluid Mech.* **14**, 189–212.

Manley, T. O. & Hunkins, H. 1985 Mesoscale eddies of the arctic ocean. *J. Geophys Res.* **90** (C3), 4911–4930.

Maxworthy, T. 1997 Convection into domains with open boundaries. *Ann. Rev. Fluid Mech.* **29**, 327–371.

Maxworthy, T. & Narimousa, S. 1994 Unsteady, turbulent convection into a homogeneous, rotating fluid, with oceanographic applications. *J. Phys. Oceanogr.* **24**, 865–887.

McWilliams, J. C. 1985 Submesoscale, coherent vortices in the ocean. *Rev. Geophys.* **23**, 165–182.

Morison, J., McPhee, M., Curtin, T. & Paulson, C. 1992 The oceanography of leads. *J. Geophys. Res.* **97** (C7), 11199–11218.

Morton, B. R., Taylor, G. I. & Turner, J. S. 1956 Turbulent gravitational convection from maintained and instantaneous sources. *Proc. R. Soc. Lond.* A **234**, 1–23.

NOH, Y., FERNANDO, J. S. & CHING, C. Y. 1992 Flows induced by the impingement of a two-dimensional thermal on a density interface. *J. Phys. Oceanogr.* **22**, 1207–1220.

RICHARDS, J. M. 1963 Experiments on the motion of isolated cylindrical thermals through unstratified surroundings. *Intl J. Air Water Poll.* **7**, 17–34.

ROUSE, H., YIH, C.-S. & HUMPHREYS, H. W. 1952 Gravitational convection from a boundary source. *Tellus* **4**, 201–210.

SCORER, R. S. 1957 Experiments on convection of isolated masses of buoyant fluid. *J. Fluid Mech.* **2**, 583–594.

SPEER, K. G. & MARSHALL, J. 1995 The growth of convective plumes at seafloor hot springs. *J. Marine Res.* **53**, 1025–1057.

STOTHERS, R. B. 1989 Turbulent atmospheric plumes above line sources with an application to volcanic fissure eruptions on the terrestrial planets. *J. Atmos. Sci.* **46**, 2662–2670.

TAYLOR, G. I. 1917 Motion of solids in fluids when the flow is not irrotational. *Proc. R. Soc. Lond.* **93**, 99–113.

TURNER, J. S. 1973 *Buoyancy Effects in Fluids*. Cambridge University Press.

WHITEHEAD, J. A., MARSHALL, J. & HUFFORD, G. E. 1996 Localized convection in rotating stratified fluid. *J. Geophys. Res.* **101**, 25705–25721.

WOODS, A. W. 1993 A model of the plumes above basaltic fissure eruptions. *Geophys. Res. Lett.* **20**, 1115–1118.

WOODS, A. W. & BUSH, J. W. M. 1999 The dynamics and dimensions of megaplumes. *J. Geophys. Res.* (in press).

WRIGHT, S. J. & WALLACE, R. B. 1979 Two-dimensional buoyant jets in a stratified fluid. *Proc. ASCE, J. Hydraul. Div.* **105** (HY11), 1393–1406.